International Journal of Architectural, Civil and Construction Sciences
ISSN: 2415-1734
Vol:9, No:8, 2015

An Analytical Study of FRP-Concrete Bridge Superstructures

Wael I. Alnahhal

***Abstract*—**It is a major challenge to build a bridge superstructure that has long-term durability and low maintenance requirements. A solution to this challenge may be to use new materials or to implement new structural systems. Fiber Reinforced Polymer (FRP) composites have continued to play an important role in solving some of persistent problems in infrastructure applications because of its high specific strength, light weight, and durability. In this study, the concept of the hybrid FRP-concrete structural systems is applied to a bridge superstructure. The hybrid FRP-concrete bridge superstructure is intended to have durable, structurally sound, and cost effective hybrid system that will take full advantage of the inherent properties of both FRP materials and concrete. In this study, two hybrid FRP-concrete bridge systems were investigated. The first system consists of trapezoidal cell units forming a bridge superstructure. The second one is formed by arch cells. The two systems rely on using cellular components to form the core of the bridge superstructure, and an outer shell to warp around those cells to form the integral unit of the bridge. Both systems were investigated analytically by using finite element (FE) analysis. From the rigorous FE studies, it was concluded that first system is more efficient than the second.

***Keywords*—**Bridge superstructure, hybrid system, fiber reinforced polymer, finite element analysis.

I. Introduction

IT is well known that bridges deteriorate with age. Because there is a large volume of bridges that were built in the 1960's (the interstate era), bridges will require increasing future maintenance, major rehabilitation, or in some cases replacement to maintain the integrity of the Nation's highway system. Longer design life structures, using the latest material and design technologies, are needed so that the nation can maintain a functional transportation network, provide longer service life, and improve the safety of the highway network. Recently, attention has been focused on FRP as alternative bridge materials. In spite of all these advantages, FRP composites have higher initial costs than conventional materials used in infrastructure application. To overcome this obstacle and to make the best use of materials, the idea of combining FRP composites with conventional construction materials such as steel and concrete has been considered by several researchers. Hillman and Murray [1] proposed the innovative idea of a hybrid FRP-concrete structural system for flexural members, which led to the concept of hybrid beam (HB). Bakeri and Sunder [2] presented an innovative structural concept for hybrid FRP-concrete bridge deck systems. The proposed deck system was a simply curved membrane of FRP filled with concrete. The idea was to use the FRP in tension and the concrete in compression. Saiidi et al. [3] presented an experimental and analytical study of hybrid beams that consist of graphite/epoxy (G/E) sections and reinforced concrete slabs. Deskovic et al. [4] investigated the short-term behavior of hybrid FRP–concrete beams. A concrete layer substitutes the glass fiber reinforced polymers (GFRP) compressive flange of traditional pultruded box sections; thus, reducing the materials cost and increasing the stiffness. Erp et al. [5] proposed hybrid FRP-concrete beams for bridge applications. The weight of the hybrid beam was about one-third that of the corresponding concrete beam. Alnahhal et al. [6] developed and tested one-quarter-scale model of an 18-m long hybrid concrete-FRP bridge superstructure. The results clearly indicate that the use of FRP in combination with concrete has led to stiffness enhancements of over 35%.

In this study, two hybrid FRP-concrete bridge superstructures were investigated analytically by using FE analysis. Both systems were investigated to select the most efficient one.

Wael I. Alnahhal is an assistant professor with the Depart. of Civil and Arch. Eng. @ Qatar University, Doha, Qatar, P. O. Box 2713 (phone: +974-4403-4197; fax: +974-4403-4172; e-mail: wael.alnahhal@qu.edu.qa).

II. The Proposed FRP-Concrete Bridge Systems

In this study, two hybrid FRP-concrete bridge systems were investigated by using FE analysis. The first system consists of trapezoidal cell units forming a bridge superstructure. The second one (system II) is formed by arch cells. The two systems rely on using cellular components to form the core of the bridge superstructure, and an outer shell to wrap around those cells to form the integral unit of the bridge. To evaluate the two systems, a bridge superstructure was designed as a simply-supported single span one-lane bridge with a width of 4.267 m (15 ft). The bridge has a length of 18.288 m (60 ft). System I is comprised of trapezoidal cross-sections surrounded by an outer shell as shown in Fig 1. According to [7], thin walled box sections are the most efficient structural forms for beams. A thin layer of concrete is placed in the compression zone of section. Concrete was confined by glass fiber reinforced polymers (GFRP) laminates that protect it from the environmental exposure. Moreover, the concrete layers reduce the local deformation of the top surface of the bridge under concentrated loads that represent truck wheel loads. Trapezoidal box sections with an inclination angle helps to reduce shear force at the interface of two box sections. According to [8], the inclination of 3/8 has the smallest deformation at the riding surface. Thus, inclination of 3/8 was chosen for the proposed bridge system. The thickness of the concrete layer is a key design parameter to optimize the hybrid structural system. According to [8], concrete can be used

efficiently to increase the flexural rigidity until the concrete thickness equals about 10% of the bridge depth. Therefore, the thickness was chosen as 99 mm, which is 8.5% of the total depth of the bridge. This proposed bridge system has several inherent advantages over all-composite bridge which can be summarized as follows:

- GFRP is corrosion-resistant and the concrete is not exposed to the environment: the system will require less maintenance than conventional bridges.
- Concrete is designed to be always in compression in the longitudinal direction. The fact that concrete is not used in the tension side leads to significant weight reduction when compared to a concrete-filled FRP tube design.
- It has been reported that the local deformation under a loading point may become large for all-composite bridge decks [2], [9]. A layer of concrete can reduce this local deformation of the top flange.

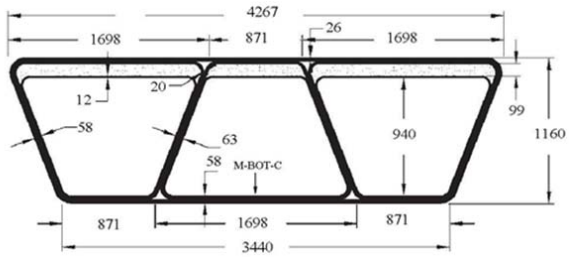

Fig. 1 Cross Section of the Hybrid FRP-Concrete Superstructure-System I (dimension in mm)

System II is formed by two components: arch cells and rectangular with semi-circular cells. Each arch cell is formed by two semicircular laminates, and in between the concrete is placed. Moreover, the rectangular with semi-circular cell is formed by two rectangular with semi-circle laminates, and in between the concrete will be placed as shown in Fig. 2. This design has several inherent advantages:

- The circular shape used in this system avoids stress concentrations that are present at the corners of I and box sections.
- The proposed design develops shell action in the transverse direction that is extremely important to ensure adequate transverse rigidity.

Table I shows the stacking sequence and thickness of different layers of both bridge systems (I and II).

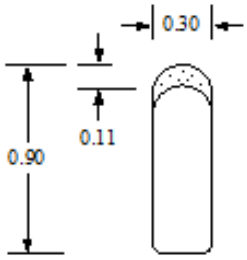

(a) Rectangular with Semi-Circular Unit Cell

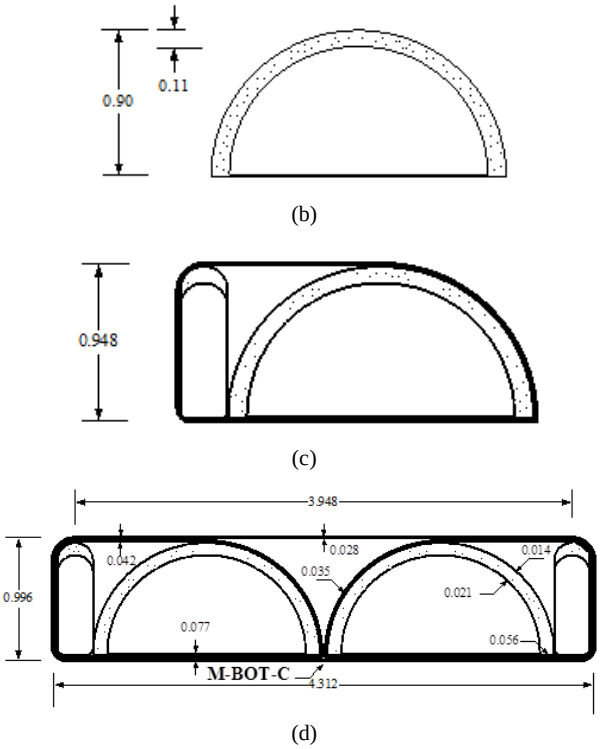

Fig. 2 System II of the Hybrid FRP-Concrete Superstructure: (a) Rectangular with Semi-Circular Unit Cell, (b) Arch Unit Cell, (c) Two- Cell subassembly, and (d) Bridge Deck Formed by Two subassemblies. (Dimensions in m)

TABLE I
THICKNESS AND STACKING SEQUENCE OF DIFFERENT LAYERS OF SYSTEMS I AND II

	System I		System II	
	Stacking Sequence	Thickness (mm)	Stacking Sequence	Thickness (mm)
Inner Tube Laminate	$[0^o_2]$	13	$[0^o_3]$	21
Outer Tube Laminate	$[0^o(45^o)_2]$	22.3	$[0^o_2]$	14
Outer-Most Tube Laminate	$[0^o_4]$	29.7	$[45^o_2]$	14
Cover Tube Laminate	------	------	$[0^o_4]$	28

An optimization of the concrete layer thickness for System II was not taken into account in this study. Instead, the effects of concrete thickness on various properties were examined as shown in Fig. 3. These properties are: (a) total weight; (b) flexural rigidity; and (c) specific flexural rigidity. The specific flexural rigidity is defined as flexural rigidity divided by weight per unit length. These properties are normalized with respect to those obtained for the case of FRP-only system. It is clear that as the concrete thickness increases, both the weight and the flexural rigidity increases. But the rate of concrete increase is higher than the rate of flexural rigidity increase. Therefore, the specific flexural rigidity decreases as the concrete thickness increases. It can be observed also that the rate of the increase in flexural rigidity is decreased when concrete thickness equal to about 9.75% of the bridge depth.

Thus, the thickness was chosen as 960 mm, which is 9.75 % of the total depth of the bridge.

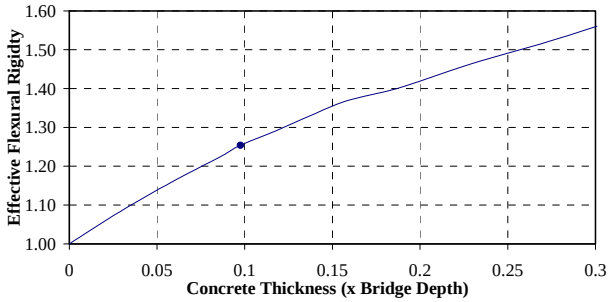

(a) Effective Flexural Rigidity

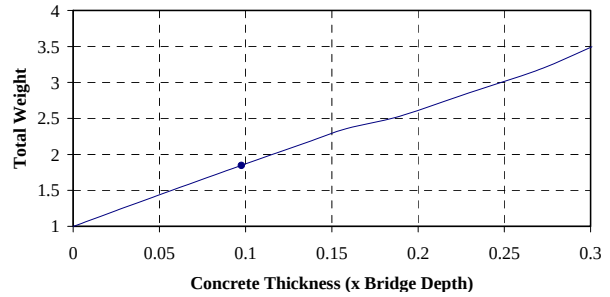

(b) Total Weight

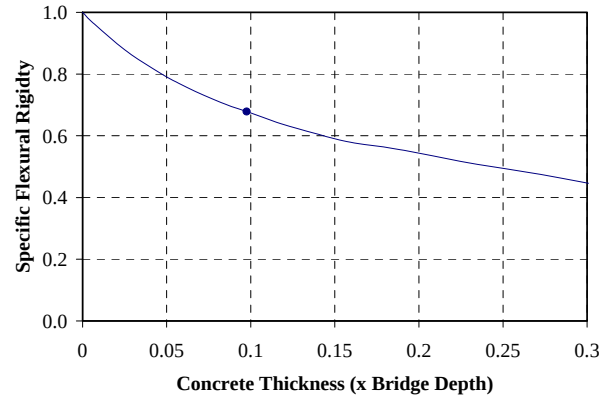

(c) Specific Flexural Rigidity

Fig. 3 Effects of Concrete Thickness on (a) Effective Flexural Rigidity, (b) Total Weight, and (c) Specific Flexural Rigidity (●: current design)

III. Loads

The AASHTO LRFD [10] specifications were used to design the proposed structural systems. Only dead and live load were considered in this study.

A. Dead Loads

The dead loads acting on the bridge are modeled either as the dead load of structural and non-structural elements, which is denoted as DC, or dead load of wearing surfaces and utilities, which are denoted as DW. The wearing surface load is 0.305 kPa.

B. Live Loads

The vehicular live load is designated as HL-93 and is comprised of a combination of the design tandem or design truck along with the design lane load. The design tandem is also a truck with a pair of (110 kN/m) axles spaced 1.2 m apart. The design lane load is a uniform load with a magnitude of 9.3 kN/m applied over a 3 m wide strip. The design truck load is three axles with loads of 145 kN, 145 kN, and 35 kN. The spacing between the 145 kN axles varies from 4.3 m to 9 m. Load configuration of these loads are shown in Fig. 4. The distance from the one support to the rear axle of a vehicle, which is denoted as d, is chosen to produce the maximum effect for deflection or moment. Table II shows the distance, d, to produce either the maximum deflection or the maximum moment.

TABLE II
DISTANCE FROM THE SUPPORT AT Y=0 TO THE REAR AXLE

		Truck		Tandem	
		(*m*)	(× Span)	(*m*)	(× Span)
Maximum Moment	Location of Rear Axle	5.57	0.305	8.24	0.451
	Location of Max. Moment	9.87	0.540	9.44	0.516
Maximum Deflection	Location of Rear Axle	6.36	0.348	8.54	0.467
	Location of Max. Moment	9.12	0.4999	9.14	0.500

IV. Design Criteria

Two design criteria are considered in designing the hybrid FRP-concrete superstructure bridge. First, we consider the stiffness criterion that includes a limit on maximum vertical displacement. The second criterion is strength, which includes first ply failure of the structure, buckling, and shear failure.

A. Deflection Criteria

It is recommended in AASHTO LRFD Bridge Design Specifications [10] that the maximum deflection under live loads needs to be smaller than L/800 (L: span length). For the live load deflection calculation, the deflection should be taken as the larger of:

- (1+IM) × design truck alone
- 25% of (1+IM) × design truck load and lane load.

where IM is dynamic load allowance and has a value of 0.33 in this case. The load case for (1+IM) × truck load was used in this study to check the serviceability condition because it produced a larger displacement than the other case. The span (L) of the hybrid bridge is 18.288 m. The maximum deflection under (1+IM) × truck load has to be smaller than 22.9 mm (L/800).

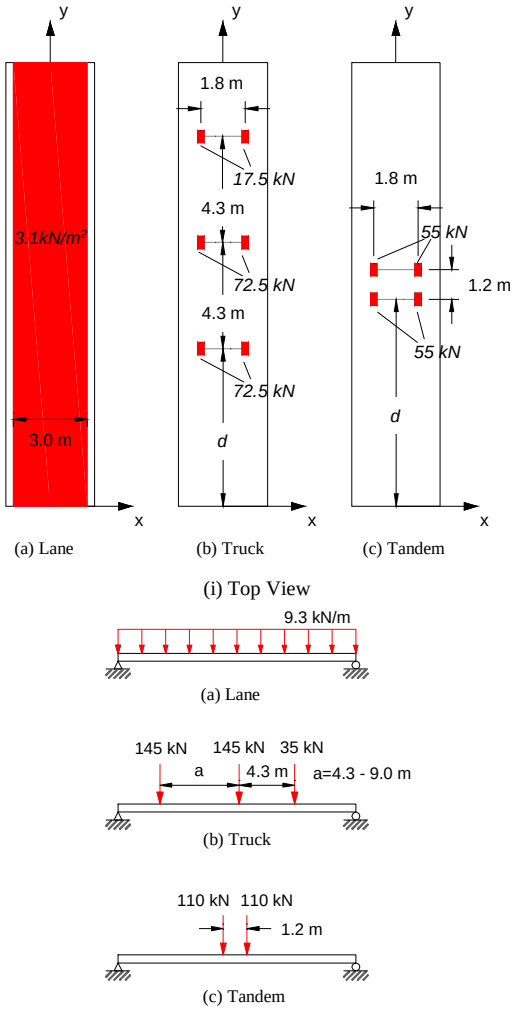

Fig. 4 HL-93 Vehicle Loading Configuration

The load combination of the service I limit is specified as [10]:

$$DC + DW + LL \quad (1)$$

where, in this study,

$$LL = LANE + (1 + IM) \times TRUCK$$

DC: Dead load of components and attachments; *DW*: Dead load of wearing surfaces and utilities; *LL*: Live load effect; *LANE*: Design lane load; *TRUCK*: Design Truck; *IM*: Dynamic allowance factor.

This service limit state refers to the load combination relating to the normal operation use of the bridge. It also relates to deflection control of the bridge design and crack control of concrete.

B. Strength Criteria

The load combination for the strength I limit is specified as [10]:

$$1.25Dc + 1.5DW + 1.75\,LL \quad (2)$$

All the force effects due to this condition are required to be under strengths of different failure modes such as flexure, shear, and buckling. No part of the GFRP should experience any ply failure.

V. Finite Element Model

For a detailed FE analysis of the hybrid FRP-concrete bridge superstructure, the finite element calculations were performed using ABAQUS [11].

A. Material Properties and Modeling

The FRP laminates are constructed using E-glass in the form of a woven fabric because of relative cost saving when compared to other forms of fibers. Vinyl ester resin is chosen as the matrix because of its high durability, and extremely high corrosion resistance. The mechanical properties of the GFRP composite material were provided for the finite element analysis by An-Cor Industrial Plastics, Inc. Table III depicts the material properties of GFRP that are utilized in the finite element models. Normal weight concrete is used in this study. The mechanical properties of concrete used in this study are presented in Table IV. The linear FE analysis can predict the behavior of the hybrid bridge with enough accuracy if the strain induced in the materials is within the strain range where the elastic moduli of the materials were computed. Both concrete and GFRP behave nonlinearly in a higher strain range. However material nonlinearity of these materials will not considered in the FEA in this study. A typical linear model for both GFRP laminates and concrete is used in this study. GFRP laminates were modeled by a four-node shell element (S4R5), while concrete was modeled by a general 3D solid element (C3D8). Fig. 5 shows the finite element model for both bridge Systems I and II.

B. Boundary Conditions

Boundary conditions were imposed on two lines of nodes of the bottom surface. Nodes at y =0 and z =0 were restrained in the y and z directions, and nodes at y =L and z =0 were restrained in the z direction. In addition, nodes at x =0, z =0, and y =0 and L were restrained in the x direction.

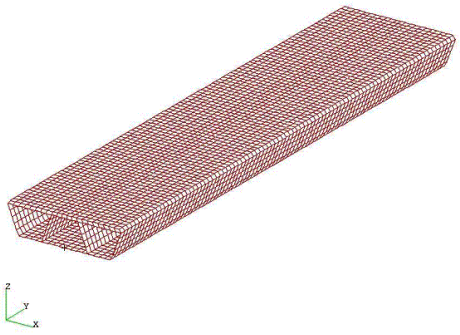

(a) System I

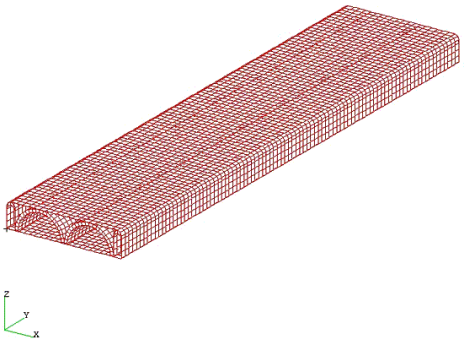

(b) System II

Fig. 5 Finite Element Models for Systems I and II

TABLE III
MECHANICAL PROPERTIES OF GFRP

Mechanical Property	Fill	Warp
Young's Modulus (GPa)	18.6	18.6
Poisson's Ratio	0.1348	0.1348
Ultimate Compressive Strength (MPa)	-241	-241
Ultimate Tensile Strength (MPa)	288	288
Ultimate Shear Strength (MPa)	56.1	56.1

C. An Analysis of Discretization Error

To obtain a FE analysis solution and a measure of the error in that solution, a series of analyses with increasing levels of refinement were performed for both systems. Convergence of the FE solution is obtained for both systems (I and II), and the refined meshes are then used in the linear static analyses. Dead load was applied to both systems (I and II). Fig. 6 shows that the discretization error in both systems (I and II) converges to zero, which is a good indication of the accuracy of their finite element mesh.

TABLE IV
MECHANICAL PROPERTIES OF CONCRETE

Mechanical Property	Value
Young's Modulus (GPa)	24.822
Poisson's Ratio	0.18
Compressive Strength, f_c' (MPa)	24.65

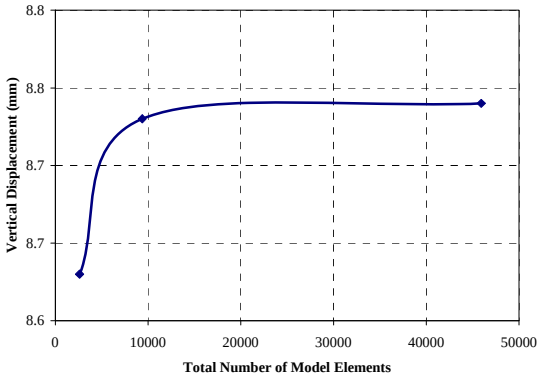

(a) System I

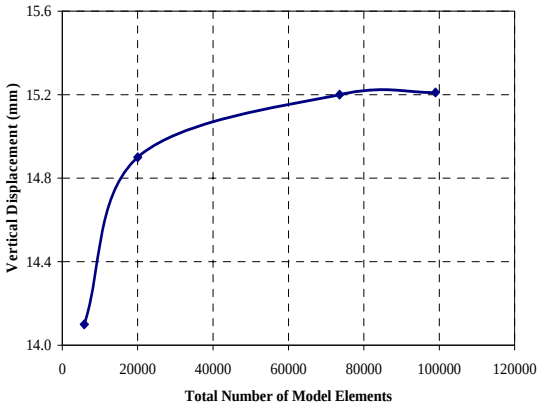

(b) System II

Fig. 6 Vertical Displacement at Mid-Span vs. Total Number of Model Elements

VI. LINEAR STATIC FINITE ELEMENT ANALYSIS

A. Deflection Criteria

To check whether the maximum deflection under (1+IM)× truck load is smaller than L/800 (22.9 mm), the load equivalent to (1+IM) ×truck load was applied to both systems (I and II). The maximum vertical displacement was 12.9 mm (0.563 ×L/800) for bridge system I, and was 13.8 mm (0.603 ×L/800) for bridge system II as shown in Fig. 7. Both systems have much smaller deflection than the deflection limit of 22.9 mm. With further design refinements, one can reduce the weight and consequently bring the maximum deflection closer to (L/800).

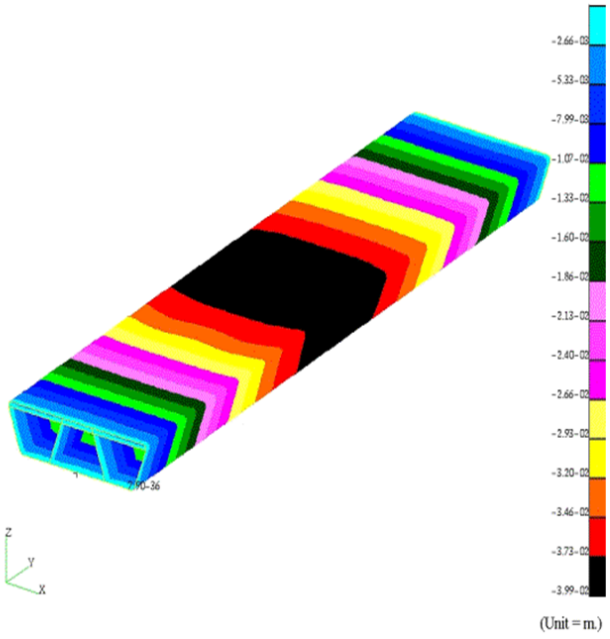

(a) System I

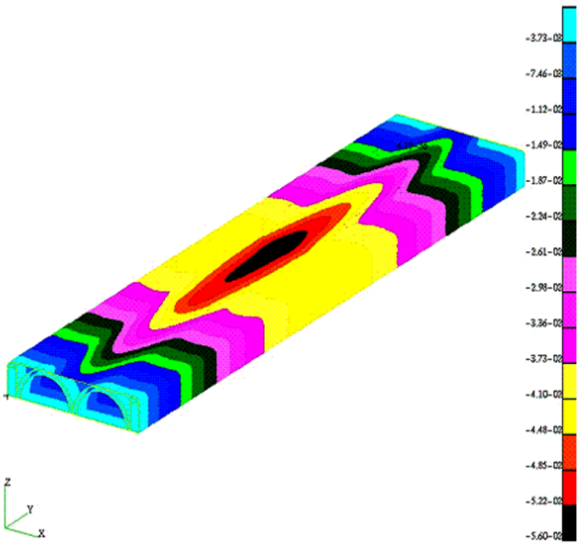

(b) System II

Fig. 7 Vertical Displacement Contours for the deflection Limit for Bridge System I & II

B. Service I Limit

The load combination for the service I limit described in (1) was applied to both bridge systems (I and II). The maximum vertical displacement was 25.2 mm (1.1 × L/800) for bridge system I. and was 29.3 mm (1.279 ×L/800) for system II. Moreover, System II has local deformation under truck load especially at the middle-top surface of the bridge superstructure as shown in Fig. 8. The maximum local vertical displacement at this area reaches 36.6 mm. Filling materials at area between two arches and the top-middle surface is recommended to overcome the local deflection.

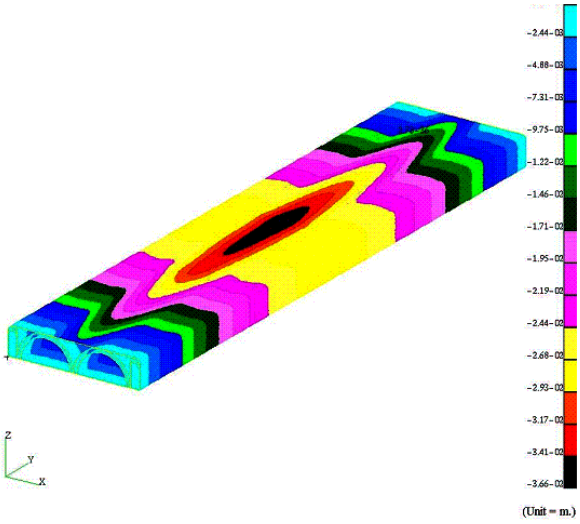

Fig. 8 Vertical Displacement Contours for the Service I Limit for Bridge System II

The Tsai-Hill criterion appears to be much more applicable to failure prediction for E-glass/Epoxy composite material than maximum stress or maximum strain failure criteria [12]. Hence, the Tsai-Hill failure criterion was used as a measure of failure of the FRP laminates in this study. The Tsai-Hill failure equation is shown in (3)

$$\left(\frac{\sigma_1}{X_1}\right)^2 - \frac{\sigma_1\sigma_2}{X_1X_1} + \left(\frac{\sigma_2}{X_2}\right)^2 + \left(\frac{\sigma_6}{X_6}\right)^2 = 1 \quad (3)$$

where X_1: Strength in the principal 1 direction; σ_1: Stress in the principal 1 direction; X_2: Strength in the principal 2 direction; σ_2: Stress in the principal 2 direction; X_6: Shear strength; σ_6: Shear stress.

It can be observed from the service I limit analysis that the maximum Tsai-Hill failure index for GFRP laminates in both bridge systems is well below 1.0. The maximum Tsai-Hill index for GFRP laminates in System I is 0.0316, and it is 0.0529 for System II. Also, we observed that the stress concentration is induced at edge corners of bridge System I, and the maximum Tsai-Hill index for GFRP laminates at these corners is 0.157. There are no stress concentrations in bridge System II. Stress concentration can be avoided at edge corners of System I by adding a vertical diaphragm at the edge near the support. The safety factor when considering the first ply failure can be obtained as

$$R = \sqrt{\frac{1}{I_{TH}}} \quad (4)$$

where I_{TH}: The maximum Tsai-Hill index in the entire structure.

The compressive stresses of concrete elements are all smaller than its compressive strength limit ($0.8\times f_c^{'}$), in both bridge systems (I and II). The maximum compressive stress of concrete elements of System I is 5.79 MPa ($0.235\times f_c^{'}$), which is located at the top of the concrete layer right under the tire area of the second axle. The maximum compressive stress in the concrete elements of System II is 8.23 MPa ($0.334\times f_c^{'}$), which is located at the top surface of the arch unit cell at the mid-span of bridge superstructure. The maximum tensile stresses of concrete in bridge system I is 2.65 MPa ($0.847 \times f_r^{'}$) which is located at the bottom of the concrete layer right under the tire area of the second axle; the maximum tensile stresses in the System II is 8.23 MPa ($2.63\times f_r^{'}$) which exceeds the tensile strength of concrete located at the bottom surface of the arch unit cell at the mid-span of the bridge superstructure. When the tensile stress exceeds the tensile strength, cracks will form.

The maximum transverse shear stress at the interface between two trapezoidal box sections in System I is 1.4 MPa which is much smaller than shear strength of commercially

available resins that range from 10.35 to 34.5 MPa [13].

C. Strength Check

The load combination for the strength I limit described in (2) was applied to both bridge systems. The maximum vertical displacement was 39.9 mm (1.74 × L/800) for bridge system I and was 44.8 mm (1.956 ×L/800) for System II. System II also has local deformation under truck load especially near the middle-top surface of the bridge superstructure. The maximum local vertical displacement at this area reaches 56.0 mm.

The maximum Tsai-Hill failure index for GFRP laminates in both bridge systems is well below 1.0. The maximum Tsai-Hill index for GFRP laminates in System I is 0.0491 and 0.075 for System II at the bottom surface of the bridge superstructure where the two-cell subassemblies are connected. Also, we observed that the maximum Tsai-Hill index for GFRP laminates reaches at these corners about 0.245 due to stress concentration. The maximum transverse shear stress at interface between two trapezoidal box sections in system I is 2.2 MPa which is much smaller than shear strength of commercially available resin. The compressive stress in the concrete elements is smaller than the compressive strength limit ($0.8\times f_c^{'}$): 9.38 MPa ($0.38\times f_c^{'}$) in System I located at the top of the concrete layer under the tire area of the second axle and 12.9 MPa. ($0.52\times f_c^{'}$) in System II is located at the top surface of the arch unit cell at the mid-span of bridge superstructure.

D. Flexural Loading Test

Both bridge systems were analyzed to examine their flexural behavior. The flexural loading configuration simulates the tandem load specified in the AASHTO LRFD Bridge Design Specifications [10]. Figs. 9 and 10 show the deformed shapes of the bottom and top surfaces of Systems I and II, under different load levels. It is apparent from these figures that System I is stiffer than system II.

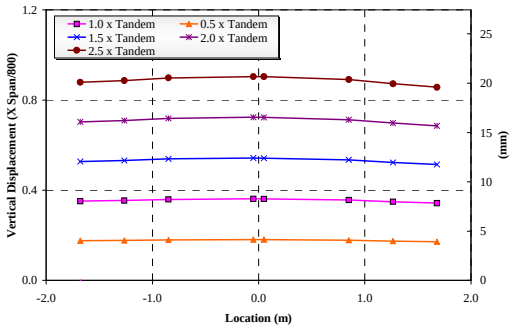

(a) Bottom Surface

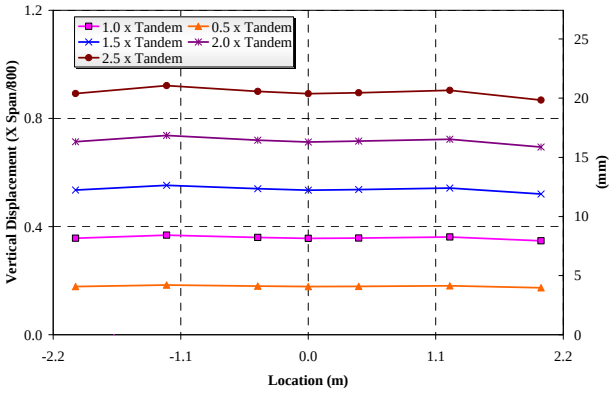

(b) Top Surface

Fig. 9 Deformed Shapes at Different Load Levels for System I

Table V enables a comparison of results from the deflection check analysis, the service I limit analysis as well as the strength I limit analysis between bridge system I and system II. Table VI enables a comparison of weight between both hybrid FRP-concrete systems. System I is lighter than System II, and stronger and stiffer than System II.

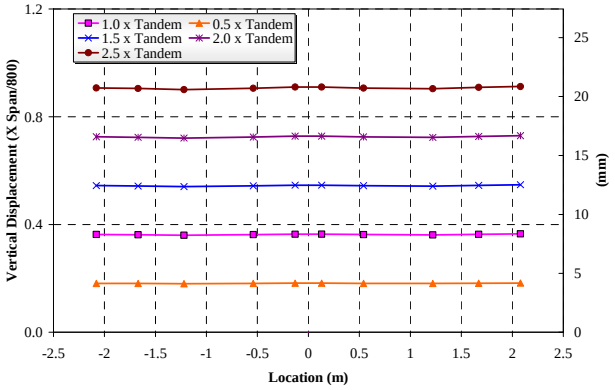

(a) Bottom Surface

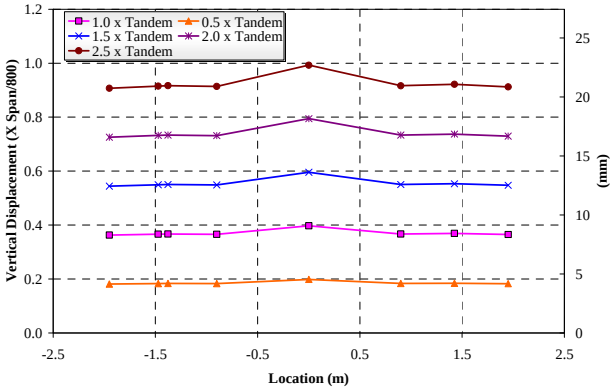

(b) Top Surface

Fig. 10 Deformed Shapes at Different Load Levels for System II

From these results, it can be concluded that System I is

more efficient than System II and System I has used to investigate the feasibility of the FRP-concrete structural systems in the reminder of the study.

TABLE V
COMPARISON OF SELECTED FEA RESULTS OF SYSTEM I AND II

		System I	System II
Deflection Check	Max. Deflection (L/800)	0.563	0.603
Service I Limit	Max. Deflection (L/800)	1.1	1.279
	Max. Tsai Hill Failure Index	0.0316	0.0529
	Safety Factor	5.63	4.35
Strength I Limit	Max. Deflection (L/800)	1.74	1.956
	Max. Tsai Hill Failure Index	0.0491	0.0653
	Safety Factor	4.51	3.91

TABLE VI
COMPARISON OF TOTAL WEIGHT OF SYSTEMS I AND II

	Weight (Tons)		
	GFRP	**Concrete**	**Total**
System I	27.77	18.01	45.82
System II	27.77	23.59	51.36

VII. CONCLUSION

In this study, two hybrid FRP-concrete bridge systems were investigated. The first system consists of trapezoidal cell units forming a bridge superstructure. The second one is formed by arch cells. The two systems rely on using cellular components to form the core of the deck system, and an outer shell to warp around those cells to form the integral unit of the bridge. Both systems were investigated analytically by using FE analysis. From the rigorous FE studies, it was concluded that first system is more efficient than the second.

REFERENCES

[1] Hillman, J. R. and Murray, T. M. (1990), "Innovative Floor Systems for Steel Framed Buildings," Mixed Structures, Including New Materials, Proceedings of IABSE Symposium, Brussels, Belgium, Vol. 60, IABSE, Zurich, pp. 672-675.
[2] Bakeri, P. A. and Sunder, S. S. (1990), "Concepts for Hybrid FRP Bridge Deck Systems," Serviceability and Durability of Construction Materials, Proceedings of the First Materials Engineering Congress, Denver, Colorado, August 13-15, 1990, ASCE, Vol. 2, pp. 1006-1015.
[3] Saiidi, M., Gordaninejad, F., and Wehbe, N. (1994), "Behavior of Graphite/Epoxy Concrete Composite Beams", Journal of Structural Engineering, Vol. 120, No. 10, pp. 2958-2976.
[4] Deskovic, N., Triantafillou, T. C., and Meier, U. (1995), "Innovative Design of FRP Combined with Concrete: Short-Term Behavior", Journal of Structural Engineering, Vol. 121, No. 7, pp. 1069-1078.
[5] Van Erp, G. (2002a), "Road Bridge Benefits from Hybrid Beams", Reinforced Plastics, Vol. 46, No. 6, Elsevier Science Ltd., Oxford, UK.
[6] Alnahhal, W., and Aref, A.J (2008), "Structural performance of hybrid fiber reinforced polymer-concrete bridge superstructure systems", Journal of Composite Structures, v 84, n 4, pp 319-336.
[7] Ashby, M. F. (1991), "Overview No.92 – Materials and Shape", Acta Metallurgica et Materialia, Vol. 39, No. 6, pp. 1025-1039.
[8] Kitane, Y. and Aref, A. (2004), "Static and fatigue testing of hybrid fiber-reinforced polymer-concrete bridge superstructure", Journal of Composites for Construction, Vol. 8, No. 2, pp. 182-190.
[9] Aref, A. J., and Parsons, I. D. (1999), "Design Optimization Procedures for Fiber Reinforced Plastic Bridges", Journal of Engineering Mechanics, Vol. 125, No. 9, pp. 1040-1047.
[10] American Association of State Highway and Transportation Officials, (2007), AASHTO LRFD Bridge Design Specifications, Second Edition, AASHTO, Washington, D.C.
[11] 3DS Dassault Systems, Inc. (2014), ABAQUS/Standard User's Manual, Version 6.14, 3DS Dassault Systems, Inc.
[12] Jones, R. M. (1999), Mechanics of Composite Materials, 2nd Edition, Taylor & Francis Inc., Philadelphia, PA.
[13] Aref, A. J. (1997), A Novel Fiber Reinforced Composite Bridge Structural system, Ph.D. Dissertation, the University of Illinois at Urbana-Champaign.